Application of eddy currents to the inspection of fatigue-corroded railway axles

Michele CARBONI [1]

[1] Department of Mechanical Engineering, Politecnico di Milano; Milano, Italy
Phone: +39 02 23998253, Fax: +39 02 23998202; michele.carboni@polimi.it

Abstract

Recent experience with existing railway axles indicates that even when they are operated within the design loads, failure can happen due to the synergetic effect of both corrosion and cyclic loads. This synergy is not yet thoroughly understood, however a need for detecting corrosion-fatigue during service is mandatory.

In the present paper, corrosion-fatigue tests are carried out, in the lab, on small-scale specimens in order to investigate the possibility to apply eddy currents non-destructive inspection to the detection of corrosion pits and corrosion-fatigue cracks during the service of railway axles. The obtained results are also supported by suitable numerical simulations carried out by a dedicated software package. Part of the presented results were obtained in the frame of the international research project RSSB T728 (just concluded) and the European research project WOLAXIM (still in progress).

Keywords: eddy currents, corrosion-fatigue, railway axles, numerical simulation

1. Introduction

During the in-service life of railway axles, fatigue is a major process resulting in structural degradation and failure. Considering the application of the damage tolerance design approach to railway axles, Zerbst et al. [1] enumerated the critical points to be considered. In particular, the present author gave contributions about the in-air crack growth properties of different steels [2] and their statistical description [3] and the influence on inspection intervals of Probability of Detection (POD) curves of the adopted Non-destructive Testing (NDT) techniques [4].

Recent experience with existing axles indicated that also corrosion is a key factor that must be addressed if maintenance costs are to be managed within acceptable limits and if the structural reliability of the axles is to be guaranteed [5-6]. Even when the axles are operated within the design loads, failure can happen due to the synergetic effect of both corrosion and cyclic loads. This synergy is not yet thoroughly understood and there is a need to derive environmentally assisted crack growth rate data, to define inspection intervals criteria and to develop proper NDT procedures for in-service maintenance, especially considering that the phenomenon is not yet considered in any relevant design standard for axles. In recent papers [7-8], the author clearly indicated that the presence of a mild aggressive environment, as artificial rainwater, is able to significantly enhance fatigue crack growth, decreasing dramatically the lifetime of railway axles. In [8] the author also analyze the pit-to-crack transition and the crack propagation mechanism in order to describe and predict the corrosion-fatigue crack growth data using a modified Murtaza and Akid model [9].

The present paper describes the investigations, carried out during a recent international scientific collaboration (RSSB T728) and an ongoing European Project (WOLAXIM), on the possibility to apply eddy currents non-destructive inspection to the detection of corrosion pits and corrosion-fatigue cracks during the service of railway axles. In particular, the carried out small-scale experimental tests are described together with the application of eddy currents (ET). It is worth remembering that the railway industry systematically relies on ultrasonic

testing (UT) and magnetic particles (MPI) to detect initiation and propagation of fatigue cracks at press-fit seats and transitions and no inspection for surface damage is systematically applied. The application of ET is then particularly suited for the problem, especially considering that it is highly innovative for the field and can be fully automated. The obtained results and different aspects about the application of ET to corrosion-fatigue of railway axles are also investigated and validated by means of numerical simulations carried out by the dedicated software package CIVA v. 10.0b [10].

2. EXPERIMENTAL TESTS ON SMALL-SCALE SPECIMENS

The aim of corrosion-fatigue tests carried out on small-scale specimens was to obtain a set of fatigue corroded specimens interrupted at fixed percentage of the estimated life [7-8] in order to: i) study the evolution of the surface damage by means of optical and scan electron (SEM) microscopes; ii) inspect the interrupted specimens by means of ET.

2.1. Experimental set-up

Tests were carried out using hour-glass round specimens (Fig. 1a) machined from retired axles made of A1N steel, a typical grade adopted for axles production. Specimens were then polished by emery paper up to P1000 grit and electro-polished to remove a 40 μm layer.
Specimens were subjected to four points rotating bending conditions (Fig. 1b) by proper facilities (maximum nominal moment equal to 35 Nm) arranged for tests in corrosive environment. Tests were carried out at a rotating speed equal to 8-10 Hz representing a service speed of about 80-100 km/h and allowing the right interaction time between fatigue and corrosion.

(a)

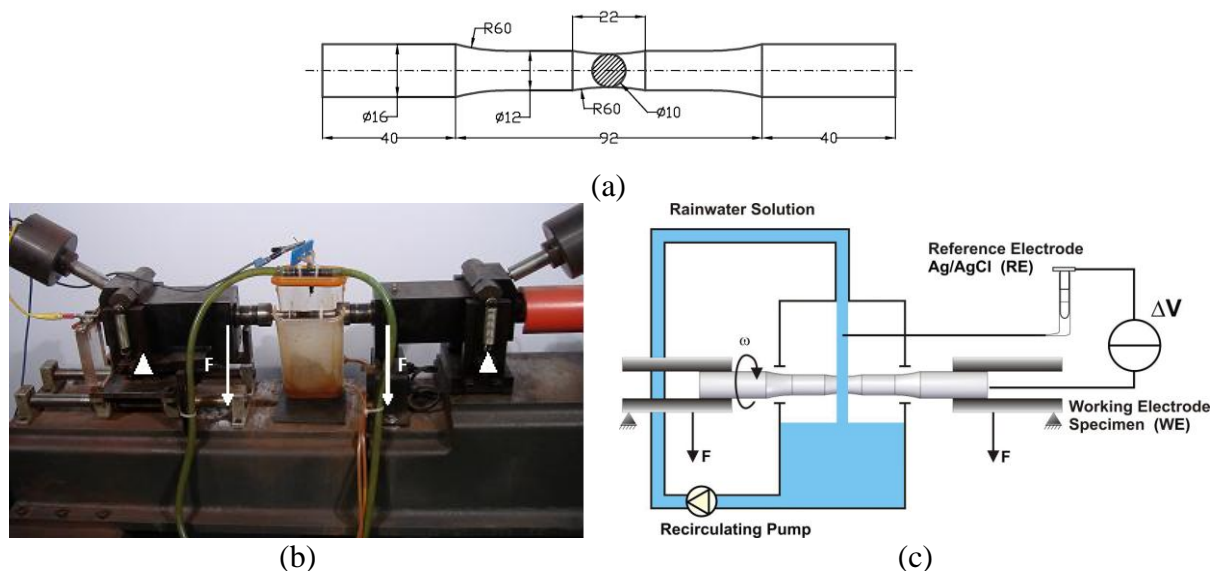(b)   (c)

Figure 1. Experimental set-up for small-scale tests: a) specimen; b) four points rotating bending facility; c) scheme of the test bench.

The corrosion environment was continuously applied to the hour-glass region of the specimens pouring the artificial rainwater solution [11] by means of a dedicated dropping system (Fig. 1c). The solution was characterized by pH=6. During the tests, the corrosion potential, the electrical conductibility, the temperature and the pH value were continuously monitored and kept constant, see [7-8] for more details.

The test plan is shown in Figure 2 and consisted in ten tests interrupted at different percentage (from 10% to 90%) of the estimated corrosion-fatigue life [7-8] considering the application of a constant amplitude load characterized by a stress range equal to 400 MPa (i.e. significantly lower than the in-air fatigue limit range of the material, equal to 500 MPa). In particular, all the specimens were initially inspected by ET before any corrosion-fatigue was applied in order to take picture of their starting condition. Then, specimens from ML2 to ML9 were interrupted at the last three 10% percentages following the schedule plan, removing the rust by slightly applying emery papers, applying the ET and starting the test again. At the final interruption, after ET inspection, the surface of the hour-glass regions was also observed at the SEM. ML10 was tested interrupting the tests at every 10% of the estimated life, while ML11 was interrupted only at 90% of the estimated life.
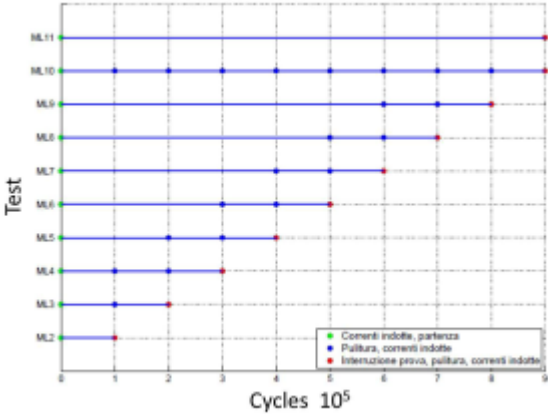

Figure 2: Test plan for small-scale specimens.

2.2. Development of corrosion-fatigue damage

In order to facilitate the final observations at the SEM, all the specimens were slightly yielded, by a mono-axial facility in order to open the cracks, and chemically cleaned following the ASTM G1-03 standard [12]. Figure 3a shows a detail of the surface of the specimen interrupted at the 10% of the estimated life.

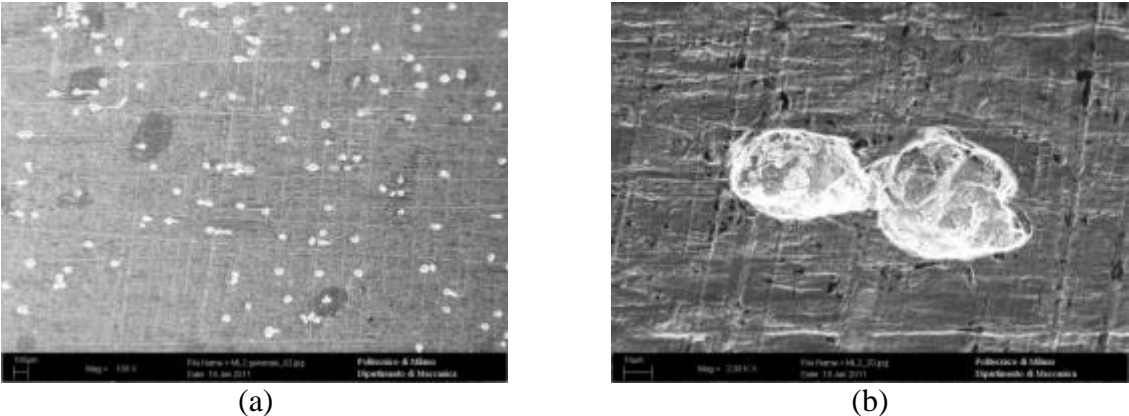(a)   (b)

Figure 3: SEM observation of the specimen interrupted at 10% of the estimated life: a) 100x; b) detail at 2000x.

As it can be seen, wide spread corrosion pits are evident, while no crack could yet be observed (Fig. 3b). Considering, instead, the specimen interrupted at 20% of the estimated life (Fig. 4a), cracks begin to develop from pits with a propagation direction perpendicular to the

applied load. Figure 4b reports a detail with an example of a corrosion pit, of a corrosion pit with an initiating crack and of a developed crack. It is also worth remarking that a coalescence of cracks emanating from pits could be observed in some regions of the specimen.

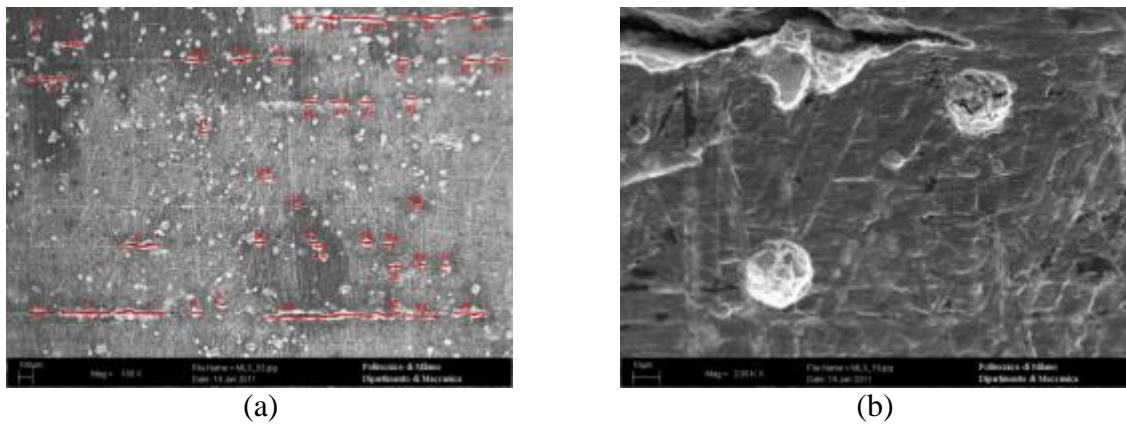(a)   (b)

Figure 4: SEM observation of the specimen interrupted at 20% of the estimated life: a) 100x; b) detail at 2000x.

Finally, as an example of the developed coalescence phenomenon, Figure 5 shows the observation of the specimen interrupted at 60% of the estimated life. As it can be seen, the dimension of corrosion-fatigue cracks increases with the considered percentage of the estimated life, while their number decreases supporting the presence of a coalescence phenomenon [13]. This damage pattern resulted to be very similar to that observed on axles retired from service [5].
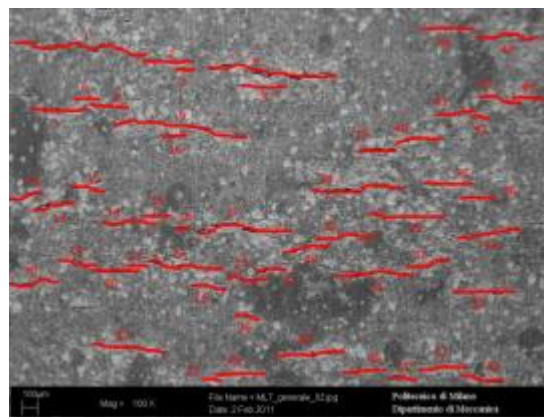

Figure 5: SEM observation of the specimen interrupted at 60% of the estimated life (100x).

2.3. ET inspection

Eddy current measurements were carried out by means of a Nortec 1000S+ control unit together with both an absolute probe characterized by a working frequency range from 500 kHz to 1000 kHz and a differential one with a working frequency range from 500 kHz to 2000 kHz. In order to apply the probes to the specimens, a dedicated frame with a special probe holder was designed and realised (Fig. 6).
The frame allowed to always keep the same position of the probe with respect to the specimen, while the repeatability of the lift-off was guaranteed adopting a contact inspection configuration where the contact was always maintained by the total weight of the probe and of the probe holder. Finally, the calibration of the working frequency was carried out using an artificial known defect located on a specimen made of A1N steel and spanning the full range

of possible frequencies, for the given probe, looking for the maximum sensitivity in terms of the biggest diameter of the circumference circumscribed to the polar response read form the control unit. It resulted that the absolute probe had to be operated at 500 kHz, while the differential one at 620 kHz.

(a)   (b)

Figure 6: Application of the ET probes to small-scale specimens.

The measurements consisted in the acquisition of the eddy current response along a complete circumferential revolution (360°) of the specimens: this means that all the prospective cracks were longitudinally inspected. The rotational speed of the specimens during ET inspections was set to 1 rpm.

Figure 7 shows the comparison of the module trends, for both the probes, in terms of the diameter of the circle circumscribed to the ET polar response. Every dot of the plots is obtained from one of the specimens interrupted at a given percentage of the estimated life. It is worth noting that for both the probes, at 0 cycles the impedance variation was different from zero: this could be ascribed to the intrinsic material micro-structural dishomogeneities. Moreover, both the probes showed the same trend, with the number of cycles, consisting in two distinct zones: the first one, ending at a number of cycles corresponding to about 40-50% of the total lifetime, showed an increasing impedance variation due to the formation of pits and initiation of cracks; the second one showed, instead, a sort of saturation, suggesting a nearly constant response with the increment of cycles. Finally, the differential probe seems to be systematically more sensible than the absolute one.
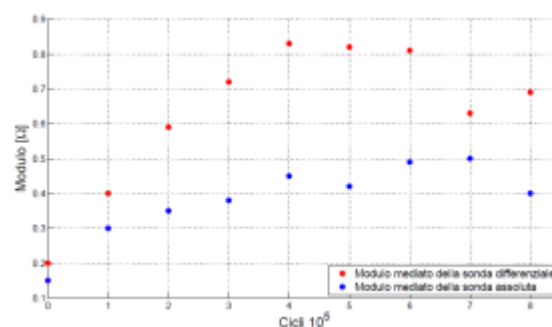

Figure 7: Module trends for the absolute and the differential probes applied to small-scale specimens.

An experimental explanation of the observed saturation was given checking how many corrosion-fatigue cracks are contemporary inspected. In particular, the inspection radius of the absolute probe was firstly determined using a cracked C(T) specimen made of A1N steel (Fig. 8a): the crack was inspected longitudinally with the same set-up and ET parameters used during the experimental tests. The inspection radius was defined as the distance from the center of the probe to the crack tip when no influence was anymore observed in the ET polar diagram. Such distance resulted to be equal to 2.06 mm and the inspected area is reported on a

SEM observation of the surface of a small-scale specimen in Figure 8b. As it can be seen, multiple cracks are inspected contemporary and it could be concluded that: i) at the beginning of the test, few small cracks are influencing the ET response, while when the number of cracks increases a saturation is reached due to the very complicated features of the cluster; ii) numerical or analytical modeling of ET inspection of corrosion-fatigue problems seems to be very complicated.

| (a) | (b) |

Figure 8: Inspection radius of the ET absolute probe: a) experimental determination by a cracked C(T) specimen; b) comparison of the inspection radius with the corrosion-fatigue damage pattern.

3. NUMERICAL SIMULATION OF EDDY CURRENT TESTING

In order to interpret and understand some of the obtained experimental results, numerical simulations were carried out by means of the dedicated software package CIVA[nde] v.10.0b [10]. Only the absolute probe was considered in this part of the research because CIVA did not allow to properly model the geometry of the adopted differential one. Moreover, although the general geometry of the absolute probe coil was derived by a reverse engineering procedure based on radiography and optical microscopy, the details are not provided here due to the proprietary nature of the information. Numerical simulations were carried out considering a 50x50x5 mm panel made of a general carbon steel similar to A1N grade (electrical conductivity σ=6.2 MS/m and magnetic permeability μ =200 H/m, [14-15]) instead of the real cylindrical geometry which is not available in CIVA.

Some preliminary analyses were carried out in order to calibrate and verify the model before starting with the applicative simulations. First of all, the sensitivity of the numerical probe was checked in terms of normalised impedance as a function of the working frequency (Fig. 9a, where R [Ω] is the resistance of the coil, X [Ω] the reactance of the coil and X_0 [Ω] the reactance of the coil in air). The maximum sensitivity of a given probe-material couple is reached when the ratio R/X_0 is maximum [16] and it could be possible to observe that the best working frequency for the numerical probe was found to be about 500 kHz, a value very similar to the one experimentally determined (see Section 2.3), suggesting a good numerical modelling of the steel grade.

A second check was done comparing, firstly, the trend of the standard penetration depth calculated using its traditional approximated expression [14], applied to the present case, with the data available [17] in the literature (Fig. 9b). As it can be seen (red line in the figure), the trend is very close to the one expected for steel. Eventually, a numerical simulation of the electrical field [V/m] in the piece was carried out, using CIVA, for two different working frequency (20 kHz and 500 kHz) and the results were compared with the analytical results (Fig. 9c and d). As it can be seen, a very good agreement was found between the numerical simulations and the analytical values (δ=0.101 mm at 20 kHz and δ=0.0203 mm at 500 kHz), so suggesting again a good numerical modelling of the probe.
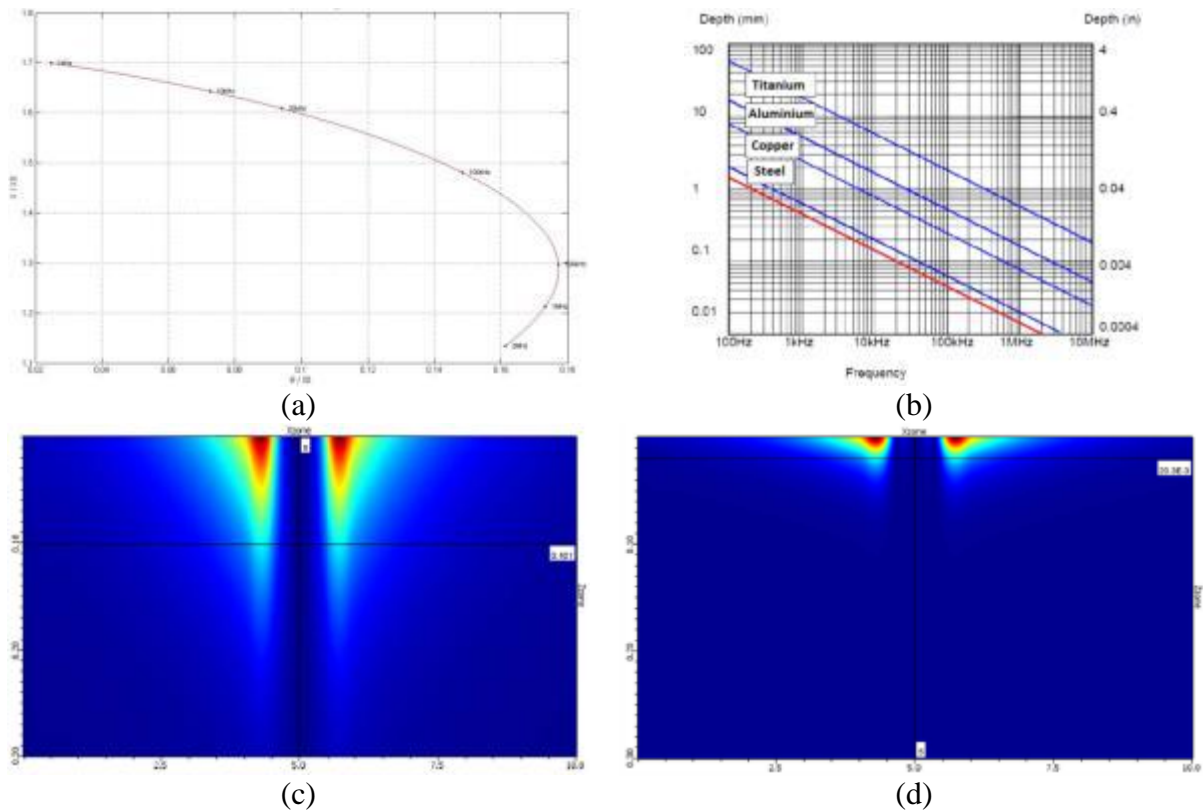
(a)   (b)

(c)   (d)

Figure 9: Calibration of the numerical model: a) sensitivity analysis; b) comparison of the numerical standard penetration depth with data available in the literature; c) electrical field for working frequency equal to 20 kHz; d) electrical field for working frequency equal to 500 kHz.

It is worth noting that a working frequency equal to 20 kHz was chosen due to the order of magnitude suggested in the literature for inspecting stress-corrosion cracks [18]. Actually, stress-corrosion and corrosion-fatigue are two very different physical phenomena characterised by different damage patterns (Fig. 10) and, while some research papers are available in the literature on ET inspection of stress corrosion (see, for example, [18]), none could be found on inspection of corrosion-fatigue.
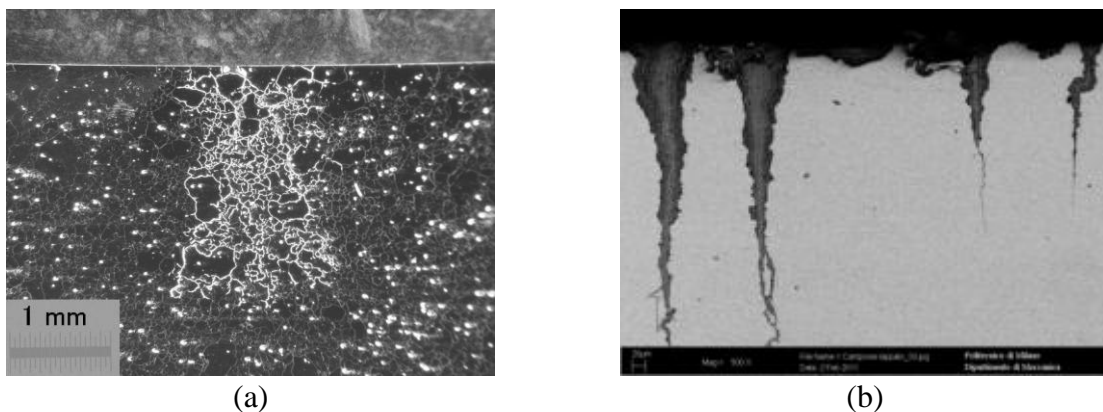

(a)   (b)

Figure 10: Comparison between damage patterns due to stress-corrosion [18] (a) and corrosion-fatigue (b).

The evidence of corrosion-fatigue damage shown in Figure 10b was obtained by a longitudinal lapped section obtained from one of the small-scale specimens tested as

described in Section 2. As it can be seen, this kind of damage is characterised by many very shallow cracks (maximum depth equal to about 200-300 μm) wide spread on the surface of the specimen. Stress-corrosion is, instead, characterised by very deep cracks (Figure 10a shows an example taken from [18] were the crack is 2-3 mm deep) having a very complicated geometrical morphology. The comparison between the two characteristic damage patterns and the electrical fields shown in Figure 9 allows to conclude that the optimum working frequency is completely different between stress-corrosion and corrosion-fatigue: in order, for the eddy currents, to invest the whole cracks, the former should be inspected with deeper electrical fields, obtained by lower working frequencies, as in Figure 9c, while the latter with less deep electrical fields obtained by higher working frequency (Fig. 9d).

The last check dealt with the inspection radius. The already described cracked C(T) specimen (Section 2.3) was experimentally inspected considering different working frequencies from 500 kHz to 1 MHz and determining the inspection radius. Eventually, dedicated numerical simulations were carried out in order to compare the experimental inspection radii with the numerical ones. In particular, the current intensity was determined on the surface of the numerical panel and the distance from the centre of the probe to where such intensity is no more influenced looked for. Figure 11a shows the example for frequency equal to 500 kHz, while Figure 11b shows the comparison between experiments and numerical simulations for the considered frequency range. As it can be seen, the inspection radius increases linearly with incrementing the working frequency and the correlation between experiments and numerical analyses is very good.
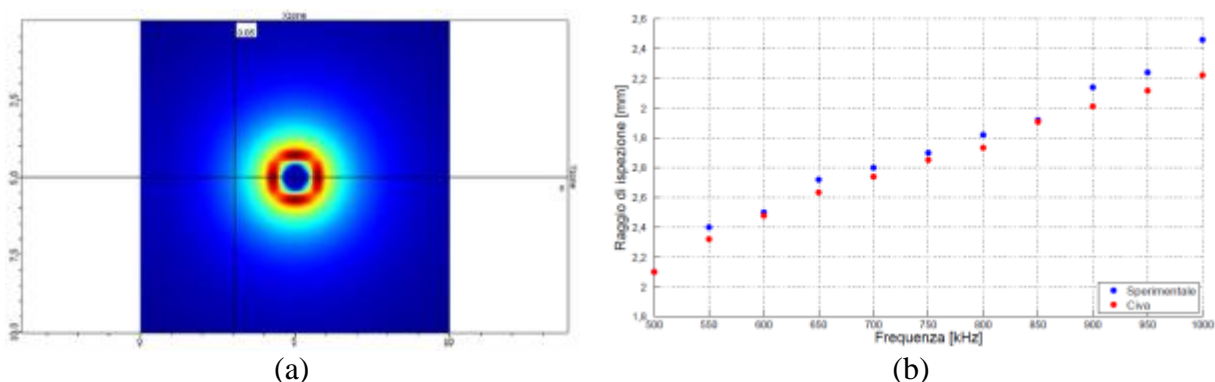

Figure 11: Analysis of the inspection radius: a) electrical field in the case of 500 kHz; b) comparison between experimental and numerical results.

The first application of the calibrated numerical model dealt with the validation of the adopted longitudinal scanning direction of corrosion-fatigue cracks. In particular, a single crack was introduced in the numerical panel and then longitudinally and transversely inspected (Fig. 12a and b, respectively) by the 500 kHz probe. As it can be seen from the polar diagrams (Fig. 12c and d for the longitudinal and transverse scans, respectively), the phase is very similar for the two scanning directions (-43° for the transversal one, -49° for the longitudinal one), while the modules are significantly different: 1.072 mV for the transversal one and 3.77 mV for the longitudinal one, so supporting the choice of the experimental longitudinal inspection. The same conclusions could be drawn considering the 20 kHz probe.

The second application of the numerical model consisted in the ET inspection of crack clusters as those observed on small-scale specimens (Fig. 13a). In particular, seven simulations were run considering the fifteen longest cracks (a higher number of cracks could not be considered due to computational times) measured from each of the specimens from ML3 to ML9, i.e. those containing cracks. Such cracks were modelled considering a depth equal to 0.02 mm and a width of 0.04 mm and were introduced in the numerical steel panel

keeping the exact experimental disposition (Fig. 13b). Figures 13c and d show the trend of the ET responses for the experimental and the numerical inspections, respectively. These diagrams cannot be directly compared because of significant differences: a round specimen vs. a flat panel, the presence of oxides in the experimental cracks (Fig. 10b) absent in the numerical ones and a different output of the experiments ([mV]) and the numerical simulations ([Ω]). However, it is worth noting that the trends are qualitatively very similar, suggesting the usefulness of numerical simulations in predicting the ET response of crack clusters.
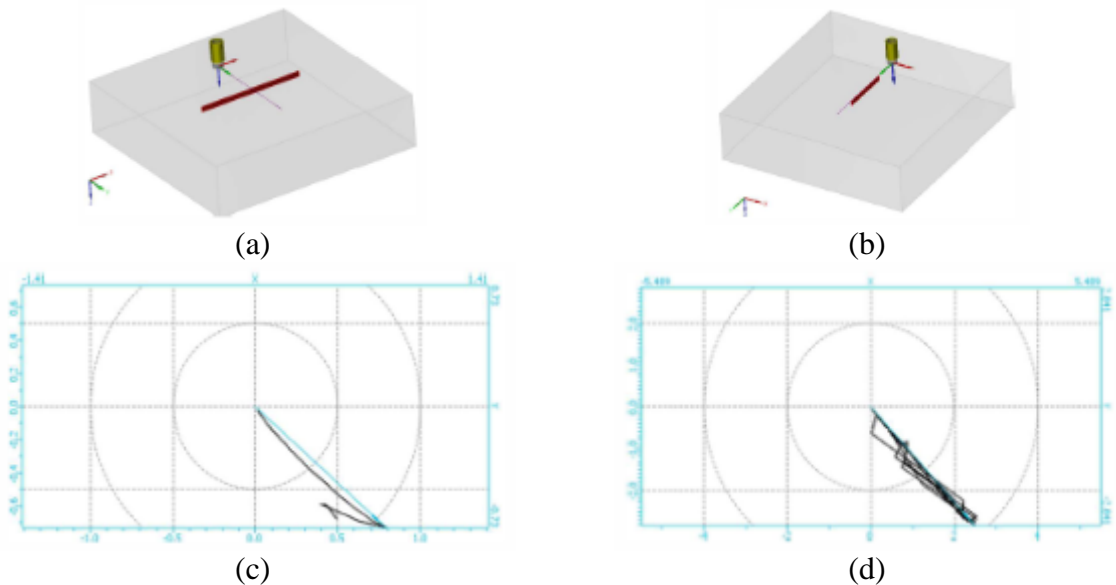

(a)   (b)

(c)   (d)

Figure 12: Evaluation of the optimum scanning direction of a crack.

(a)   (b)

(c)   (d)
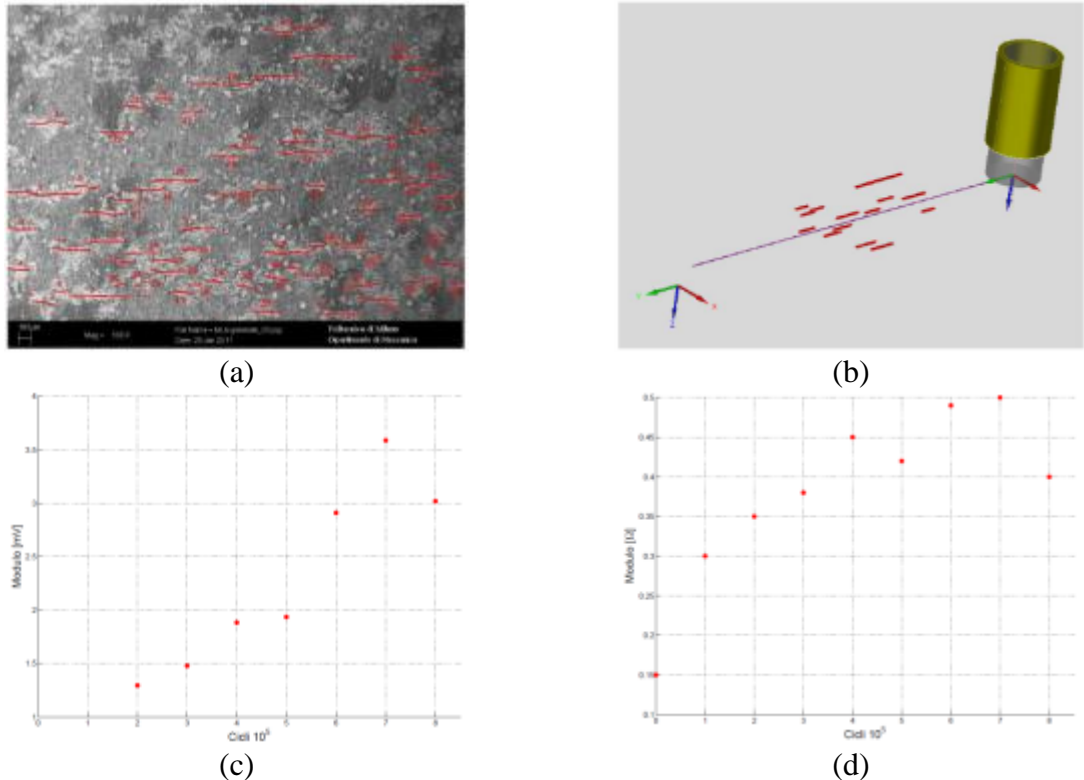
Figure 13: Simulation of ET response of crack clusters: a) experimental cluster from ML6; b) numerical set-up; c) experimental results; d) numerical results.

Acknowledgements

References

1. U. Zerbst, M. Vormwald, C. Andersch, K. Mädler, M. Pfuff. "The development of a damage tolerance concept for railway components and its demonstration for a railway axle", Eng Fract Mech, 72, pp. 209–239, (2005).
2. S. Beretta, M. Carboni, S. Cantini, A. Ghidini. "Application of fatigue crack growth algorithms to railway axles and comparison of two steel grades", J Rail Rapid Transit, 218, pp. 317–326, (2004).
3. S. Beretta, M. Carboni. "Experiments and stochastic model for propagation lifetime of railway axles", Eng Fract Mech, 73, pp. 2627–2641, (2006).
4. M. Carboni, S. Beretta. "Effect of probability of detection upon the definition of inspection intervals of railway axles", J Rail Rapid Transit, 221, pp. 409–417, (2007).
5. D. S. Hoddinot. "Railway axle failure investigations and fatigue crack growth monitoring of an axle", J Rail Rapid Transit, 218, pp. 283–292, (2004).
6. Transportation Safety Board of Canada. "Main track derailment: Canadian national train No. G-894-31-14", Railway Investigation Report R01Q0010, (2001).
7. S. Beretta, M. Carboni, A. Lo Conte, E. Palermo. "An investigation of the effects of corrosion on the fatigue strength of A1N steel railway axles", J Rail Rapid Transit, 222, pp. 129–143, (2008).
8. S. Beretta, M. Carboni, G. Fiore, A. Lo Conte. "Corrosion-fatigue of A1N railway axles steel exposed to rainwater", Int J fatigue, 32, pp. 952-961, (2010).
9. G. Murtaza, R. Akid. "Empirical corrosion fatigue life prediction models of a high strength steel", Eng Fract Mech, 67, pp. 461–474, (2000).
10. CEA/CEDRAT, CIVA^{nde} 10.0b User's Manual, 2011.
11. G. Brunoro, A. Frignani, A. Colledan, C. Chiavari. "Organic films for protection of Copper and Bronze against acid rain corrosion", Corrosion Science, 45, pp. 2219-2231, (2003).
12. ASTM G1-03. "Standard Practice for Preparing, Cleaning and Evaluating Corrosion Test Specimens", ASTM International (2003).
13. Carboni M., Beretta S., Lo Conte A. (2011), Research on corrosion fatigue of railway axles, Insight 53, 361-367.
14. NDT Resource Center. http://www.ndt-ed.org. 2010.
15. The Physics Factbook. http://hypertextbook.com. 2011.
16. T.Sollier, F.Buvat, G. Pichenot, D. Premed. Eddy current modeling of ferrite-cored probes, application to the simulation of eddy current signals from surface breaking flaws in austenitic steel. Proc. 16th World Conf. on NDT, Montreal 2004.
17. Joseph M. Buckley. An introduction to eddy current testing theory and technology. Technical report, 2007.
18. Noritaka Yusa, Stéphane Perrin, Kenzo Miya. Eddy current data for characterizing less volumetric stress corrosion cracking in nonmagnetic materials. Materials Letters, 2006.